Separation and Purification Technology 350 (2024) 127891

Contents lists available at ScienceDirect

Separation and Purification Technology

journal homepage: www.elsevier.com/locate/seppur

A reduced model for pilot-scale vacuum-enhanced air gap membrane distillation (V-AGMD) modules: Experimental validation and paths for process improvement

Kleber Marques Lisboa [a,*], Ingrid Vasconcelos Curcino [b], Abdul Orlando Cárdenas Gómez [b], Luz Elena Peñaranda Chenche [b], Renato Machado Cotta [b,c], Carolina Palma Naveira-Cotta [b]

[a] Laboratory of Thermal Sciences (LATERMO), Department of Mechanical Engineering (TEM/PGMEC), Universidade Federal Fluminense, UFF, Niterói, RJ, Brazil
[b] Laboratory of Nano & Microfluidics and Microsystems (LabMEMS), Mechanical Eng. Dept., POLI & COPPE, Universidade Federal do Rio de Janeiro, UFRJ, Rio de Janeiro, RJ, Brazil
[c] Laboratory General Directorate of Nuclear and Technological Development (DGDNTM), Brazilian Navy, Ministry of Defense, Rio de Janeiro, RJ, Brazil

ARTICLE INFO

Keywords:
Physics-based reduced model
Vacuum-enhanced air gap membrane distillation
Energy efficiency
Pilot-scale

ABSTRACT

A fast and robust computational model of a spiral-wound vacuum-enhanced air gap membrane distillation (V-AGMD) module at the pilot-scale is proposed and implemented. In contrast with data-driven models available in the literature, a physics-based approach is adopted for more reliable generalization beyond the validation dataset. A total of 86 experimental results, of which 41 are described in this work and 45 come from independent sources available in the literature, are used in the validation effort with quite favorable results. With the confidence on the robustness of the methodology due to the wide range of operational parameters and the use of spiral-wound modules of four different sizes included in the validation comparisons, a physical analysis is conducted varying the air gap pressure, the number of feedwater channels, the feedwater flow rate, and the membrane area. Improvements of up to 60% in both water productivity and energy efficiency can be achieved by intensifying the vacuum in the air gap or decreasing the number of feedwater channels. These parameters achieve performance gains due to less resistance in the air gap for vapor to migrate through it, in the former case, and a reduced temperature polarization effect, in the latter case. Smaller flow rates favor energy efficiency at the expense of water productivity by simultaneously decreasing transport-phenomena-related irreversibility and the partial pressure difference across the membrane and the air gap. In addition, this tradeoff between energy efficiency and driving force is shown to lead to an optimum value for the membrane area beyond which the permeate flow rate through the membrane starts to fall due to the small driving force. An illustrative case is predicted to achieve energy efficiency metrics, such as a gain-output ratio of 12.7, competitive with multi-effect distillation.

1. Introduction

Membrane distillation (MD) is an emerging water desalination technology based on the migration of water vapor induced by a partial pressure difference that appears when two water free surfaces at different temperatures are kept separated by a porous and hydrophobic membrane [1,2]. Allying the capabilities of dealing with high salinity brines [3–5], operating in mild pressures and temperatures [1,2], and serving as a secondary process recovering low-grade waste heat [6,7], MD has attracted much attention from researchers in the last two decades.

However, membrane distillation has lower energy efficiencies relative to other more established technologies, such as reverse osmosis (RO), multi-stage flash (MSF), and multi-effect distillation (MED) [8,9]. Reverse osmosis is the dominant technique in terms of market share [10] and its energy expenditure is deeply tied to the Gibbs free energy of separation of salt from water, which amounts to 2.7 kJ/kg [11]. On the other hand, distillation-based methods must provide around 2400 kJ/kg in thermal energy to vaporize water [12]. Even when the heat recovery and the lower exergy content of heat sources in comparison with electricity are taken into account, the comparison with RO remains unfavorable in terms of energy use [13]. Moreover, MD still lags behind other distillation techniques in terms of energy efficiency, except for small-

* Corresponding author.
E-mail address: kmlisboa@id.uff.br (K.M. Lisboa).

https://doi.org/10.1016/j.seppur.2024.127891
Received 28 January 2024; Received in revised form 27 April 2024; Accepted 7 May 2024
Available online 9 May 2024

Nomenclature

a	Height of the channel [m]
A_m	Membrane area $[m^2]$
a_w	Activity coefficient [–]
B	Permeability $[kg/m^2sPa]$
c_p	Specific heat at constant pressure [J/kgK]
D_{eff}	Effective diffusivity $[m^2/s]$
d_p	Average pore diameter of the membrane [m]
D^0_{wa}	Molecular diffusivity $[Pa.m^2]$
D^k_w	Knudsen diffusivity $[m^2/s]$
GOR	Gain-output ratio [–]
h	Heat transfer coefficient $[W/m^2K]$
h_{lv}	Latent heat of vaporization [J/kg]
j_w	Mass flux through the membrane $[kg/m^2s]$
k	Thermal conductivity of the fluid [W/mK]
k_{air}	Thermal conductivity of most air [W/mK]
k_b	Thermal conductivity of the cooling wall [W/mK]
k_g	Thermal conductivity of the air gap [W/mK]
k_l	Thermal conductivity of the distillate film [W/mK]
k_m	Thermal conductivity of the membrane [W/mK]
k_p	Thermal conductivity of the membrane polymer [W/mK]
k_s	Thermal conductivity of the spacer [W/mK]
M	Molar mass [g/mol]
$\dot{m}$	Mass flow rate [kg/s]
N_a	Molar flux of air $[mol/m^2s]$
N_w	Molar flux of water $[mol/m^2s]$
N_c	Number of channels [–]
n_d	Number of discharges [–]
Nu	Nusselt number [–]
p	Absolute pressure in the air gap [Pa]
p_a	Partial pressure of air [Pa]
p_{atm}	Atmospheric pressure [Pa]
p_{mf}	Partial pressure of vapor at the interface between the membrane and the hot feedwater [Pa]
p_{mg}	Partial pressure of vapor at the interface between the membrane and the air gap [Pa]
p_v	Vapor pressure [Pa]
p_{vac}	Vacuum pressure, $p_{vac} = p_{atm} - p$ [Pa]
p_w	Partial pressure of water [Pa]
Pr	Prandtl number [–]
q''	Heat flux $[W/m^2]$
q''_c	Conduction heat flux $[W/m^2]$
q''_v	Heat flux carried by the vapor $[W/m^2]$
$\mathscr{R}$	Universal gas constant [J/molK]
R	Thermal resistance $[Km^2/W]$
Re	Reynolds number [–]
T	Temperature [°C]
TPC	Temperature polarization coefficient [-]
u	Intrinsic velocity of the fluid within the channels [m/s]
w	Width of the channel [m]
W	Mass fraction [–]
x	Molar fraction [–]

Greek Symbols

Δt	Time interval between discharges [s]
ΔV	Volume of each discharge $[m^3]$
δ	Membrane thickness [m]
δ_b	Cooling wall thickness [m]
δ_g	Air gap thickness [m]
δ_l	Distillate film thickness [m]
ε_c	Porosity of the channel [–]
ε_s	Gap spacer porosity [–]
μ	Dynamic viscosity of the fluid [Pa.s]
ρ	Density of the fluid $[kg/m^3]$
τ	Tortuosity [–]

Superscripts and subscripts

b	Refers to the cooling wall
c	Refers to the cold feedwater channel
eq	Equivalent quantity
f	Refers to the hot feedwater channel
g	Refers to the air gap
in	Refers to the inlet
l	Refers to the distillate film
m	Refers to the membrane
out	Refers to the outlet
p	Refers to the permeate
$salt$	Refers to the dissolved salts
v	Refers to water vapor
w	Refers to water
$wall$	Quantity evaluated at the wall

scale desalination plants [9]. As MD matures, it can possibly offset this disadvantage in comparison to RO and other distillation techniques. Nevertheless, applications with available low-grade waste heat from different sources and in combination with solar energy installations are already ideal scenarios for the employment of MD [14–16].

Several membrane distillation configurations were proposed over the years. The most studied one is the direct contact membrane distillation (DCMD) that is characterized by the direct contact of both the hot feed and cold permeate streams with the membrane [14,15]. However, DCMD suffers from relatively low energy efficiency due to parasitic heat conduction losses through the membrane [17] and requires external heat exchange equipment to properly recover heat [18]. An interesting alternative is the air gap membrane distillation (AGMD). In this configuration, instead of direct contact between the cold permeate and the membrane, an additional air layer is introduced, rendering the module less conducive to heat losses [19,20]. The penalty imposed by the air gap is the increase in mass transport resistance stemming from the presence of the air-filled gap. As a result, AGMD provides smaller mass fluxes than DCMD [21], even though comparisons at the pilot scale indicate otherwise due to limits in the energy input in these situations, favoring the higher energy efficiency of AGMD [22].

Evacuation of the air gap, like the one employed in the so-called vacuum membrane distillation (VMD) [23], has been proposed to overcome this limitation with the added benefit of further reducing the conductive heat losses through the membrane [24–26]. If the total pressure within the gap is lowered but maintained above the saturation pressure of the condensate, a liquid film still forms, dispensing the need for an external condenser, as is necessary in VMD. Up to a threefold increase in the mass flux has been reported using this vacuum-enhanced air gap membrane distillation (V-AGMD) [27]. Originally, V-AGMD required a vacuum pump to actively reduce the pressure in the air gap, adding a significant burden to the capital and operational costs of the plant. However, an innovative design by Aquastill BV employed a Venturi tube at the suction of the cooling pump to impose this pressure reduction with negligible cost [28], turning this V-AGMD design into one of the most promising for commercial applications.

Many analyses of membrane distillation modules were carried out at the bench scale, whose conclusions are only partially applicable to the

pilot scale [22]; more studies on the latter scale are deemed crucial to determine the viability of membrane distillation for commercial applications [19]. In recent years, more research has been carried out involving DCMD [29], AGMD [30], and V-AGMD [28,31,32] operating at the pilot-scale. Nonetheless, these experiments are often expensive and time consuming to conduct. Experimentally validated models for those modules are then crucial for more economical and informative optimization analyses of these equipment. Models for pilot-scale operation of DCMD [29], AGMD [30], and V-AGMD [33,34] are available in the open literature. However, in the latter case, response surface models (RSM) based on experimental data were proposed and they might present problems when trying to generalize beyond the dataset. Ideally, a physics-based model should be established to better grasp how relevant parameters affect the performance of the desalination module. Furthermore, even though physics-based models for DCMD [18,29,35] and AGMD [30,36,37] modules are readily available, they require the solution of differential equations, which may be too computationally expensive for tasks such as multi-objective optimization or system-wide analyses.

The present work aims at proposing a reduced, 0D model for vacuum-enhanced air gap membrane distillation spiral-wound modules operating at pilot-scale. Mass and energy balances allied with a careful analysis of the transmembrane transport of water molecules and thermal energy are used for that purpose. Results from the model and computational code developed are compared with 86 sets of experimental data, both our own [15,16] and from independent experiments available in the literature [33], to build confidence on its robustness and accuracy across a wide range of operational and geometrical parameters. Finally, a brief physical analysis involving the effects of membrane area, number of channels, and absolute pressure at the air gap is conducted to inspect their effect on water productivity and energy efficiency.

2. Materials and methods

2.1. Experiments

Fig. 1 provides a schematic of the water desalination system PURA-1 devised by the company Aquastill BV (Netherlands) used in the experiments and as reference in the modeling effort. The instrumentation is also indicated in the same figure. A PLICA-13 vacuum-enhanced air gap membrane distillation spiral-wound module acts as the centerpiece of the system. The module itself has single inlet and outlet ports; however, internally, the feed stream is divided among six hot and cold feedwater channels, totaling twelve channels. The hot feedwater channels are sandwiched between two membranes that in turn are connected to two different sets of air gaps, cooling plates, and cold feedwater channels. The total membrane area is 12.96 m^2 and each channel has a length of 2.7 m. The hot and cold feedwater channels are kept from collapsing using 2 mm thick polypropylene spacers; spacers made of the same material but with thickness of 0.8 mm are inserted in each air gap also for structural purposes. An aluminum foil coated on both sides with polyethylene terephthalate and measuring 62 μm in thickness is used to separate the air gap from the cooling channel.

The overall circuit is capable of internally recovering both heat and water by recirculating the feed continuously, while the salinity in the feed tank is controlled by automatically adding freshwater and rejecting brine to compensate for the amount that migrated through the membranes. The permeate condensed in the air gap is collected in the permeate tank. A Venturi tube utilizes the effect of the same name, along with the suction from the cooling pump, to create vacuum in the permeate tank. This, in turn, induces vacuum within the air gaps. The heating circuit is comprised of LIRA 200 (SOLAREM, Brazil) flat plate solar collectors with a total area of 12 m^2 combined with a 300 L vertical thermal storage tank containing an immersed 5 kW electrical resistor (Kisoltec, Brazil). In the context of the present controlled experiments, the solar collectors act only as heat supplement and the transient nature

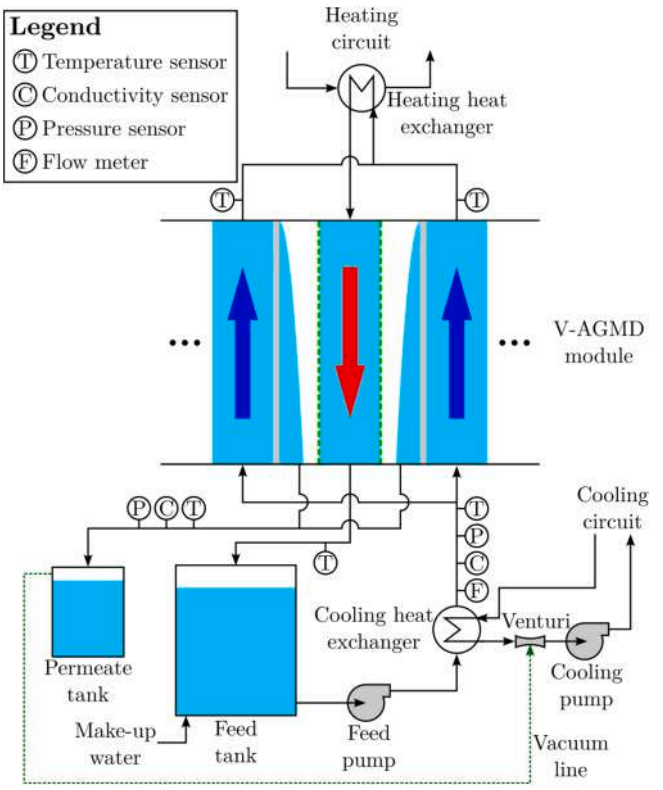

Fig. 1. Schematic of the pilot-scale apparatus. Not to scale.

of solar energy is isolated from the desalination system that operates at steady state. On the other hand, the cooling circuit leads to a cooling tower where heat is rejected from the water to the atmosphere. In each of these circuits, three-way valves and a bypass are employed to control the inlet temperatures in the channels.

The temperature at the inlet and outlet of the hot and cold feedwater channels, the pressure at the inlet of the cooling channel, and the electrical conductivity are monitored using an Esaware PLC data acquisition system (ESA Automation & Robotics, Italy). The permeate tank content is discharged by 3.4 L each time and, by recording the intervals between discharges, one can calculate the average permeate flow rate as

$$\dot{m}_p = \frac{\rho_p n_d \Delta V}{\Delta t} \tag{1}$$

where $\dot{m}_p$ is the permeate flow rate, ρ_p is the density of the permeate, n_d is the number of discharges throughout the experiment, $\Delta V \equiv 3.4L$ is the volume of each discharge, and Δt is the time interval between discharges. Once the permeate flow rate is divided by the membrane area of 12.96 m^2, the average mass flux through the membrane is obtained. Additional details of the experiments can be found in the Supplementary Information.

3. Numerical model

3.1. Hot and cold feedwater channels

The forced convection heat transfer within the hot and cold feedwater channels is accounted for by using a correlation for spacer-filled channels in the spiral-wound membrane distillation modules manufactured by Aquastill BV (Netherlands) [30]. The correlation is given by

$$\mathrm{Nu} = 0.22\mathrm{Re}^{0.69}\mathrm{Pr}^{0.13}\left(\frac{\mathrm{Pr}}{\mathrm{Pr}_{\mathrm{wall}}}\right)^{0.25} \tag{2a}$$

with dimensionless parameters defined as

$$\mathrm{Nu} = \frac{ha}{k} \tag{2b}$$

$$\mathrm{Re} = \frac{\rho u a}{\mu} \tag{2c}$$

$$\mathrm{Pr} = \frac{\mu c_p}{k} \tag{2d}$$

where Nu, Re, and Pr are the Nusselt, Reynolds, and Prandtl numbers, respectively, h is the heat transfer coefficient, a is the height of the channel (measured along the perpendicular direction to the membrane), u is the intrinsic velocity of the fluid within the channels, μ is the dynamic viscosity of the fluid, ρ is the fluid density, c_p is the fluid specific heat, and k is the thermal conductivity of the fluid. The subscript wall refers to a property evaluated at the wall, which, in the case of the hot channel, is the membrane and, in the cold channel, is the cooling plate.

The intrinsic velocity can be obtained from the mass flow rate as

$$u = \frac{\dot{m}/N_c}{\rho w a \varepsilon_c} \tag{3}$$

where $\dot{m}$ is the total mass flow rate distributed among all channels, N_c is the number of either hot or cold feedwater channels in the module, w is the width of the channel, and ε_c is the porosity of the channel.

3.2. Membrane

The effective thermal conductivity of the membrane is estimated using Maxwell's model in the form [30,38]

$$k_m = 0.93 k_{air} \frac{1 + 2\beta(1-\varepsilon_m)}{1 - \beta(1-\varepsilon_m)} \tag{4a}$$

with

$$\beta = \frac{k_p - k_{air}}{k_p + 2k_{air}} \tag{4b}$$

where k_m, k_p, and k_{air} are the membrane, membrane polymer, and moist air thermal conductivities, respectively, and ε_m is the membrane porosity.

The Dusty Gas model is employed in the analysis of the mass transport through the membrane. Neglecting surface diffusion [39] and Poiseuille-like transport [40], we then have [18]

$$\frac{N_w}{D_w^k} + \frac{p_a N_w - p_w N_a}{D_{wa}^0} = -\frac{1}{\mathscr{R} T_m} \frac{dp_w}{dx} \tag{5}$$

where N_w and N_a are respectively the molar fluxes of water and air, p_w and p_a are respectively the partial pressures of water and air, D_w^k is the Knudsen diffusivity, D_{wa}^0 is the molecular diffusivity, $\mathscr{R}$ is the universal gas constant, and T_m is the average temperature along the membrane.

Neglecting the air movement within the membrane pores [8], yields

$$\frac{N_w}{D_w^k} + \frac{p_a N_w}{D_{wa}^0} = -\frac{1}{\mathscr{R} T_m} \frac{dp_w}{dx} \tag{6}$$

Employing Dalton's law $p_a = p - p_w$, where p is the total pressure within the pores, and enforcing that N_w must be conserved through the membrane,

$$N_w = \frac{D_{wa}^0}{\mathscr{R} T_m \delta} \ln\left(\frac{D_{wa}^0 - D_{eff} p_{mg}}{D_{wa}^0 - D_{eff} p_{mf}}\right) \tag{7a}$$

with

$$D_{eff} = \frac{D_w^k D_{wa}^0}{D_{wa}^0 + p D_w^k} \tag{7b}$$

where δ is the membrane thickness, D_{eff} is the effective diffusivity, and p_{mg} and p_{mf} are the partial pressures of water vapor at the interfaces between the membrane and the air gap and the hot feedwater, respectively.

Converting the molar flux into mass flux, we have

$$j_w = \frac{M_w D_{wa}^0}{\mathscr{R} T_m \delta} \ln\left(\frac{D_{wa}^0 - D_{eff} p_{mg}}{D_{wa}^0 - D_{eff} p_{mf}}\right) \tag{8}$$

where j_w is the mass flux and M_w is the water molar mass.

Assuming the partial pressure difference along the membrane is small and that the water vapor pressure is negligible in comparison with the total pressure, eq. (8) can be simplified to

$$j_w = B_m \left(p_{mf} - p_{mg}\right) \tag{9a}$$

with

$$B_m = \frac{M_w D_{eff}}{\mathscr{R} T_m \delta} \tag{9b}$$

where B_m is the membrane permeability.

The molecular and Knudsen diffusivities can be obtained as [18,41]

$$D_{wa}^0 = 4.46 \times 10^{-6} \frac{\varepsilon_m}{\tau_m} T_m^{2.334} \tag{10a}$$

$$D_w^k = \frac{\varepsilon_m}{\tau_m} \frac{d_p}{3} \sqrt{\frac{8 \mathscr{R} T_m}{\pi M_w}} \tag{10b}$$

where $\tau_m \equiv 2.27$ [30] is the membrane tortuosity and d_p is the membrane average pore diameter.

The Antoine equation is used to evaluate the vapor pressure near liquid water free surfaces given its temperature. Mathematically [18,41],

$$p_v(T) = \exp\left(23.1964 - \frac{3816.44}{T + 227.02}\right) \tag{11}$$

where p_v is the vapor pressure and T must be in °C.

In the hot feedwater case, the presence of salts dissolved in the water alter the partial pressure in comparison to eq. (11). To account for this deviation, a correction in the form

$$p_{mf} = a_w (1 - x_{salt}) p_v \tag{12}$$

is used, where a_w is the activity coefficient and x_{salt} is the salt molar fraction in the feedwater. The activity coefficient is given by

$$a_w = 1 - 0.5 x_{salt} - 10 x_{salt}^2 \tag{13}$$

The effects of concentration polarization induced by the mass transport from the bulk fluid to the membrane surface are not considered. Instead, the bulk molar fraction is employed in eqs. (12) and (13). The salinity of the feedwater is often provided as a mass fraction that can easily be converted into the molar fraction using the following expression:

$$x_{salt} = \frac{M_w W}{(1 - W) M_{salt} + W M_w} \tag{14}$$

where W is the salt mass fraction and M_{salt} is the salt molar mass.

3.3. Air gap

The air gap in AGMD and V-AGMD applications is often slender to avoid the introduction of a strong resistance to vapor mass transport. This fact sets the air gap in the so-called tall cavity regime [42]. Therefore, one-dimensional heat conduction from the heated to the

cooled walls dominates the heat transfer phenomenon, allowing the heat flux to be written as

$$q_c'' = \frac{k_g(T_{mg} - T_{gl})}{\delta_g - \delta_l} \tag{15}$$

where q_c'' is the conduction heat flux through the air gap, k_g is the thermal conductivity of the air gap, T_{mg} and T_{gl} are the temperatures at the air–gap-membrane and air–gap-condensate-film interfaces, respectively, δ_g is the air gap thickness, and δ_l is the condensate film thickness.

The thermal conductivity of the air gap is the result of a combination of the moist air and gap spacer thermal conductivities. The parallel flux model is adopted for that purpose, which results in

$$k_g = k_{air,g}\varepsilon_s + k_s(1 - \varepsilon_s) \tag{16}$$

where $k_{air,g}$ and k_s are the thermal conductivities of the air and the gap spacer, respectively, and ε_s is the gap spacer porosity.

As in the case of the membrane, the Dusty Gas model is adopted in the analysis of the vapor mass transport through the air gap. Adding the negligible Knudsen transport mechanism to the set of hypotheses already discussed in the context of the membrane, yields

$$j_w = \frac{M_w D_{wa}^0}{\mathscr{R} T_g \delta_g} \ln\left(\frac{p - p_{gl}}{p - p_{mg}}\right) \tag{17}$$

where p_{gl} is the water vapor partial pressure at the interface between the moist air and the condensate and T_g is the average temperature within the air gap.

Performing a linearization very similar to the one that led to eq. (9a, b), eq. (17) can be rewritten as

$$j_w = B_g\left(p_{mg} - p_{gl}\right) \tag{18a}$$

with

$$B_g = \frac{M_w D_{wa}^0}{\mathscr{R} T_g p \delta_g} \tag{18b}$$

The molecular diffusivity, D_{wa}^0, is estimated using eq. (10a), but for the average air gap temperature, T_g, instead of T_m, and disregarding the effects of the porosity and tortuosity of the medium. The partial pressure p_{gl} is calculated using the Antoine eq. (11) without any correction, assuming the permeate is free of dissolved salts and other impurities.

The effect of operating with the air gap and membrane pores below the atmospheric pressure is introduced by

$$p = p_{atm} - p_{vac} \tag{19}$$

where p_{atm} is the atmospheric pressure and p_{vac} is the vacuum pressure.

3.4. Condensate film

One-dimensional heat conduction through the film is adopted, yielding

$$q'' = \frac{k_l(T_{gl} - T_{lb})}{\delta_l} \tag{20}$$

where q'' is the heat flux that crosses the whole module, k_l is the thermal conductivity of the liquid film, and T_{lb} is the temperature at the interface between the permeate and the cooling wall.

3.5. Cooling wall

The heat conduction through the cooling wall is also assumed to be one-dimensional, allowing for the heat flux to be written as

$$q'' = \frac{k_b(T_{lb} - T_{bc})}{\delta_b} \tag{21}$$

where k_b is the thermal conductivity of the cooling wall, δ_b is the wall thickness, and T_{bc} is the temperature at the interface between the wall and the cold feedwater.

3.6. V-AGMD Module

Fig. 2 presents the mass transport resistances that the distillate flux must overcome to migrate from the hot feedwater channel to the condensate film. From this circuit, an equivalent mass transport resistance can be derived as

$$R_{eq}^m = \frac{1}{B_{eq}} = \frac{1}{B_m} + \frac{1}{B_g} \tag{22}$$

where R_{eq}^m is the equivalent mass transport resistance and B_{eq} is the equivalent permeability of the membrane and the air gap.

Hence, the mass flux can be determined from solely the partial pressures of water vapor at the hot end of the membrane and at the free surface of the condensate in the following way:

$$j_w = B_{eq}\left(p_{mf} - p_{gl}\right) \tag{23}$$

The thermal resistances along the membrane distillation module are illustrated in Fig. 3. Once an equivalent thermal resistance is determined, it is easy to evaluate the heat flux through the module upon knowing the hot and cold feedwater temperatures. However, expressions for the thermal resistance offered by each compartment of the module must be available, which are established in the sequence.

Convective thermal resistance of the hot and cold feedwater channels:

$$R_f = \frac{1}{h_f} \tag{24a}$$

$$R_c = \frac{1}{h_c} \tag{24b}$$

where R_f and R_c are respectively the thermal resistances in the hot and cold feedwater channels, and h_f and h_c are respectively the heat transfer coefficients in the hot and cold feedwater channels.

Conductive thermal resistance of the membrane:

$$R_m = \frac{\delta}{k_m} \tag{25}$$

where R_m is conductive thermal resistance of the membrane.

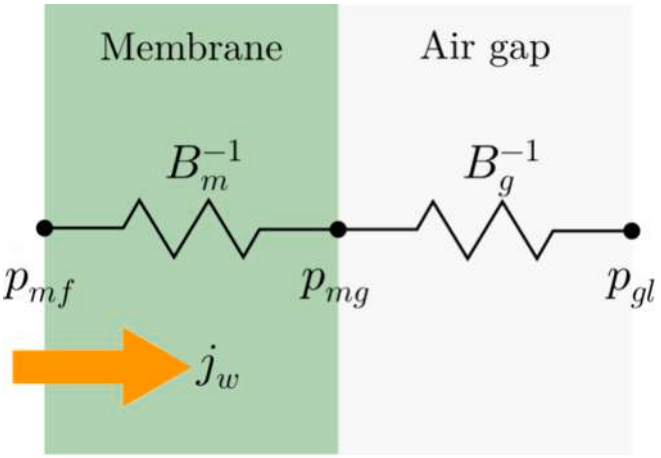

Fig. 2. Mass transfer resistances within the membrane distillation module.

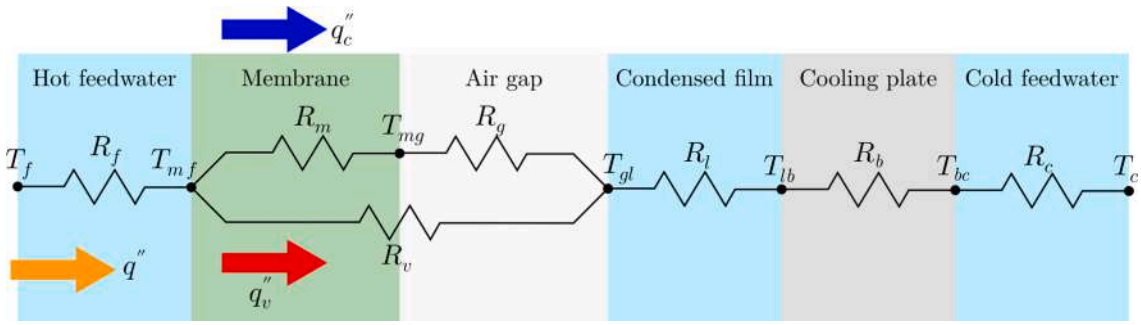

Fig. 3. Thermal resistances within the membrane distillation module.

Conductive thermal resistance of the air gap:

$$R_g = \frac{\delta_g - \delta_l}{k_g} \tag{26}$$

where R_g is the conductive thermal resistance of the air gap.

Thermal resistance of the vapor transport through the membrane and air gap:

The thermal energy carried by the vapor along the membrane and the air gap is given by

$$q''_v = j_w h_{lv} \tag{27}$$

thus,

$$R_v = \frac{T_{mf} - T_{gl}}{q''_v} = \frac{T_{mf} - T_{gl}}{j_w h_{lv}} \tag{28}$$

where h_{lv} is the latent heat of vaporization of the water and R_v is the thermal resistance of the vapor transport through the membrane and air gap.

Conductive thermal resistance of the distilled water film:

$$R_l = \frac{\delta_l}{k_l} \tag{29}$$

where R_l is the thermal resistance of the distilled water film.

Conductive thermal resistance of the condensing wall:

$$R_b = \frac{\delta_b}{k_b} \tag{30}$$

where R_b is the thermal resistance of the condensing wall.

Associating the thermal resistances in accordance with Fig. 3, the equivalent thermal resistance can be written as

$$R_{eq} = R_f + \frac{R_v(R_m + R_g)}{R_v + R_m + R_g} + R_l + R_b + R_c \tag{31}$$

where R_{eq} is the equivalent thermal resistance of the membrane distillation module.

The heat flux through the whole module can then be determined by

$$q'' = \frac{T_f - T_c}{R_{eq}} \tag{32}$$

where $T_f \equiv 0.5(T_{f,in} + T_{f,out})$ and $T_c \equiv 0.5(T_{c,in} + T_{c,out})$ are the arithmetic means between the inlet and outlet temperatures in the hot and cold feedwater channels, respectively.

Once the heat flux is obtained from eq. (32), the temperatures at the interfaces between the hot feedwater and the membrane, between the condensing wall and cold feedwater, between the condensing wall and the distillate film, and between the air gap and the distilled film can be determined respectively by

$$T_{mf} = T_f - q'' R_f \tag{33a}$$

$$T_{bc} = T_c + q'' R_c \tag{33b}$$

$$T_{lb} = T_{bc} + q'' R_b \tag{33c}$$

$$T_{gl} = T_{lb} + q'' R_l \tag{33d}$$

Deducing the heat flux due to vapor migration from the total heat flux, we then have

$$q''_c = q'' - q''_v \tag{34}$$

that, in turn, can be used to find the temperature at the interface between the membrane and the air gap as follows:

$$T_{mg} = T_{mf} - q''_c R_m \tag{35}$$

Evaluating the mass balance in the hot feedwater channel,

$$\dot{m}_{out} = \dot{m}_{in} - j_w A_m \tag{36}$$

where $\dot{m}_{in}$ and $\dot{m}_{out}$ are mass flow rates at the inlet and outlet of the hot feedwater channel, respectively, and A_m is the membrane area.

A salt mass balance in the feedwater channel yields

$$W_{out} = \frac{\dot{m}_{in}}{\dot{m}_{out}} W_{in} \tag{37}$$

where W_{in} and W_{out} are the salt mass fractions at the inlet and outlet of hot feedwater channel.

Finally, energy balances applied to both the hot and cold feedwater channels yield

$$T_{f,out} = T_{f,in} - \frac{q'' A_m}{\dot{m}_{in} c_{p,f}} \tag{38}$$

$$T_{c,out} = T_{c,in} + \frac{q'' A_m}{\dot{m}_c c_{p,c}} \tag{39}$$

where $T_{f,in}$ and $T_{f,out}$ are the hot feedwater temperatures at the inlet and outlet of the channel, respectively, $T_{c,in}$ and $T_{c,out}$ are the cold feedwater temperatures at the inlet and outlet of the channel, respectively, $\dot{m}_c$ is the cold feedwater mass flow rate, and $c_{p,f}$ and $c_{p,c}$ are respectively the hot and cold feedwater specific heats. Strictly speaking, eq. (38) should consider that the mass flow rate varies from the entry to the outlet of the hot feedwater channel. However, such variations are neglected in the energy balance context due to the fact that thermodynamics imposes that the relative difference between the inlet and outlet mass flow rates is at most 6.4% [43].

The gain-output ratio (GOR) is a useful metric to evaluate the energy efficiency of distillation equipment. In this work, it is defined as the ratio of the heat transfer rate carried through the module by the water vapor to the heat input from an external source; in this case, the heat provided

by the heating circuit in Fig. 1. Mathematically,

$$\mathrm{GOR} = \frac{j_w A_m h_{lv}}{\dot{m}_c c_{p,c}\left(T_{f,in} - T_{c,out}\right)} \tag{40}$$

The temperature polarization coefficient is defined as the ratio between the effective temperature driving force $T_{mf} - T_{gl}$ and the average bulk temperature difference between the hot and cold feedwater channels and may be written as

$$\mathrm{TPC} = \frac{T_{mf} - T_{gl}}{T_f - T_c} \tag{41}$$

where TPC is the temperature polarization coefficient.

The necessary thermophysical properties of saltwater are taken from correlations reported in [12,44], while the ones for moist air are retrieved from correlations for saturated air-water-vapor mixtures from [45].

3.7. Computational procedure

A computational code was developed using the C programming language to solve the nonlinear algebraic equations for the mass flux, outlet and interfacial temperatures, heat fluxes, and outlet salinity and mass flow rate in the hot feedwater channel. A C function that progressively calculates the mass flux using eq. (23) and the thermal resistances, using them to provide the output temperatures, salinities, heat fluxes, and flow rates is written. Newton's method with secant line search in the L_2 norm of the objective functions, implemented in the *SNES* module of the open-source *Portable, Extensible Toolkit for Scientific Computation* (PETSc) version 3.19.4 [46], is used to solve the set of nonlinear eqs. (23), (33a-d), and (35-39). The Generalized Minimum Residual (GMRES) algorithm is used for the inner linear iterations [47]. The tolerances for the inner linear and Newton iterations are respectively 10^{-12} and 10^{-10}. The code is openly available at https://github.com/labmems/vagmd0Dmodel.git to ensure that any interested reader can understand the implementation and reproduce the results.

4. Results and discussion

4.1. Model validation

At first, a comparison between the results from the numerical model and the experiments conducted as described in section 2.1 is provided. Fig. 4 illustrates the comparison of the predicted and measured mass flux (Fig. 4a) and hot and cold feedwater outlet temperatures (Fig. 4b) from which the temperature drop in the feedwater channels can be estimated. Two salinities are included in the analysis, namely 10 and 35 g/L. In the horizontal and vertical axes are respectively plotted the simulated and experimental values. Error bars stemming from a careful uncertainty analysis described in detail in the Supplementary Information are also included. A total of 41 operational conditions are simulated for the comparisons, with input values summarized in Tables 1 and 2. The vacuum pressure p_{vac} in Table 2 refers to how much below the atmospheric is the pressure within the air gap and the membrane pores, that is, $p_{vac} = p_{atm} - p$. Results in numerical form for the mass flux are also provided in Table 2.

The mass flux predicted by the computational code is consistently within the experimental error for all experimental points, which is quite remarkable, given the simplicity of the reduced model and the fact that it takes approximately 15 ms to run in an Intel i7 11800H, 64 GB DDR4 laptop. On the other hand, the outlet temperatures are biased towards an underestimation of the total heat that flows from the hot to the cold feedwater channels. Nevertheless, the absolute deviation floats between 1 and 2 °C, which is, percentagewise, small in comparison with the total temperature variation in either channel, typically in the range from 20 to 40°C. In addition, the calculated temperature deviation amounts to 20%, on average, of the temperature difference between the hot feedwater inlet and cold feedwater outlet, that is relevant for performance metrics such as the GOR. For these reasons, and considering the simplicity of the approach, the comparison with the pilot-scale experimental results is deemed satisfactory.

To further increase the confidence in the capability of the developed numerical model and associated computational code, comparisons with 45 independent experimental results from [33] employing spiral-wound V-AGMD modules manufactured by Aquastill® are made. Modules with three different sizes spanning from 7.2 m^2 to 25.92 m^2 named AS7, AS24, and AS26 are contemplated. The operational conditions are

Table 1
Geometrical and fixed parameters of the V-AGMD desalination module.

Parameter	Value	Unit	Source
Water molar mass	18.05	[g/mol]	–
Salt (NaCl) molar mass	58.443	[g/mol]	–
Atmospheric pressure	101325	[Pa]	–
Membrane area	12.96	[m^2]	Manufacturer
Number of feedwater channels	6	–	Manufacturer
Membrane thickness	100	[μm]	Manufacturer
Membrane porosity	85%	–	Manufacturer
Pore diameter	0.32	[μm]	Manufacturer
Feedwater channels thickness	2	[mm]	Manufacturer
Feedwater channels width	0.4	[m]	Manufacturer
Air gap thickness	0.8	[mm]	Manufacturer
Channel spacer porosity	79%	–	[30]
Air gap spacer porosity	84%	–	[30]
Condensing wall thickness	62	[μm]	Manufacturer
Membrane polymer conductivity	0.35	[W/mK]	Manufacturer
Spacer conductivity	0.27	[W/mK]	[48]
Condensing wall conductivity	0.35	[W/mK]	Manufacturer
Condensate film thickness	600	[μm]	Estimated

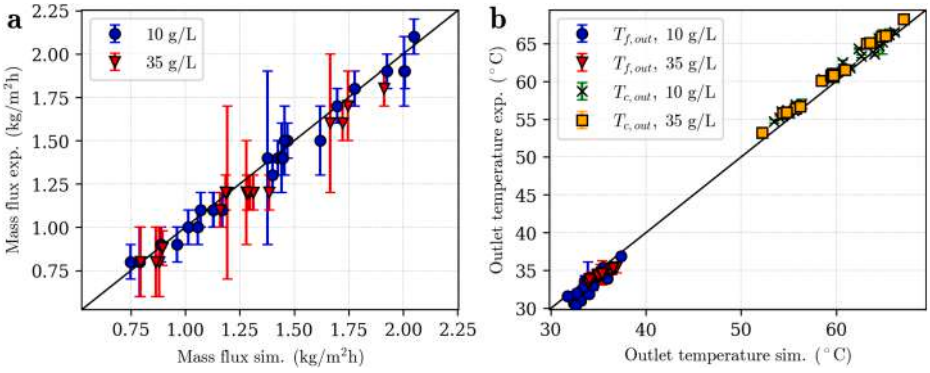

Fig. 4. Comparison of the results from the reduced model with experimental results. (a) Mass flux; (b) Hot and cold feedwater temperatures at the outlets.

Table 2
Operational parameters for the experiments with the pilot-scale V-AGMD desalination module.

Salinity: 10 g/L					**Salinity:** 35 g/L				
$T_{f,in}$ [°C]	$T_{c,in}$ [°C]	$\dot{m}_{in}$, $\dot{m}_c$ $\left[\frac{kg}{h}\right]$	p_{vac} [mbar]	j_w $\left[\frac{kg}{m^2h}\right]$	$T_{f,in}$ [°C]	$T_{c,in}$ [°C]	$\dot{m}_{in}$, $\dot{m}_c$ $\left[\frac{kg}{h}\right]$	p_{vac} [mbar]	j_w $\left[\frac{kg}{m^2h}\right]$
60	27	600	496.33	1.5	60	30	400	295.00	0.8
65	27	600	496.10	1.8	60.2	30	400	499.80	0.88
67.3	27	600	496.38	1.9	60	30	600	297.90	1.1
69.2	27	600	494.30	2.1	60	30	600	496.70	1.2
65	30	300	498.55	0.9	70	30	400	295.40	1.2
65	30	500	496.78	1.4	70.1	30	400	498.70	1.2
70	30	500	495.64	1.7	70.1	30	600	296.90	1.7
70	30	300	499.42	1.0	70	30	600	495.60	1.8
60	27.5	600	12.48	1.1	56.6	30	500	396.70	0.8
60	30	600	12.20	1.1	73.3	30	500	397.90	1.6
60	30	400	11.24	0.8	65	30	332	397.60	0.8
60	27.5	400	11.54	0.8	65	30	668	393.70	1.6
70	27.5	400	14.29	1.1	65.1	30	500	230.00	1.2
60	27.5	600	497.39	1.5	64.7	30	500	566.40	1.2
70	27.5	400	492.16	1.4	65	30	500	396.90	1.2
60.2	30	400	500.61	0.9	65	30	500	399.60	1.2
70.3	30	400	501.00	1.3	65.1	30	500	396.60	1.2
70	30	600	500.88	1.9					
60	29.9	600	502.28	1.4					
70	30	400	18.26	1.1					
70	30	600	17.05	1.5					
70	29.7	600	493.49	1.9					
70	27.6	400	502.43	1.4					
60	27.5	400	501.25	1.0					

provided in Table 3 and the remaining module characteristics can be found in Table 4 [33]. The results of the validation effort are depicted in Fig. 5a,b following the same logic adopted by Fig. 4a,b.

Once more, the mass flux comparisons are quite good, except for a few outliers. The study [33] reports only the outlet temperature of the cold feedwater and thus this quantity is the only temperature included in the comparison displayed in Fig. 5b. The temperature comparison indicates that the total heat transfer from the hot to the cold feedwater channels is underestimated, as noted in the discussion of Fig. 4b. However, the deviations are typically between 1 and 2 °C, which is acceptable given that the temperature variation in the feedwater channels is at least an order of magnitude greater.

4.2. Physical analysis

One of the main advantages of a physics-based model is that it offers the possibility of assessing a wide range of operational conditions and geometrical parameters without much effort. To leverage this capability,

Table 3
Operational conditions for the experiments reported in [33].

Case	$T_{f,in}$ (°C)	$T_{c,in}$ (°C)	**Flow rate** (L/h)
Run 1	60	20	800
Run 2	60	30	800
Run 3	80	20	800
Run 4	80	30	800
Run 5	60	25	400
Run 6	60	25	1100
Run 7	80	25	400
Run 8	80	25	1100
Run 9	70	20	400
Run 10	70	20	1100
Run 11	70	30	400
Run 12	70	30	1100
Run 13	70	25	800
Run 14	70	25	800
Run 15	70	25	800

Table 4
V-AGMD module-related parameters for the experiments reported in [33].

Parameter	AS7	AS24	AS26
Membrane area	7.2m^2	24m^2	25.92 m^2
Hot + cold feedwater channels	6 + 6	6 + 6	12 + 12
Channel length	1.5 m	5 m	2.7 m
Channel spacers porosity	0.78	0.86	0.78

a physical analysis of the effects of different physical parameters, such as the absolute pressure in the air gap, the number of feedwater channels, and the membrane area, have on the water productivity and energy efficiency of the spiral-wound V-AGMD desalination module. Unless otherwise stated, the parameters used in the analysis are taken from Tables 1 and 5.

4.3. Absolute air gap pressure

Fig. 6a presents the effect the absolute air gap pressure, p, has on the mass flux and permeate flow rate through the membrane. As expected, when the pressure is lowered, both metrics increase; indeed, they increase in the same proportion as the permeate flow rate is given by the mass flux multiplied by the fixed membrane area. A 60% increase in water productivity can be achieved by evacuating the air gap to 200 mbar of total pressure in comparison to operating in AGMD-mode, i.e., maintaining the air gap at the atmospheric pressure. Likewise, Fig. 6b demonstrates that the gain-output ratio is also significantly increased by operating at lower air gap pressures, more than doubling when the pressure is decreased from the atmospheric to 200 mbar. Both effects are due to the higher permeabilities of the membrane and the air gap as predicted by eqs. (9b) and (18b). This reduction in the mass transfer resistance provided by the operation at sub-atmospheric conditions leads to an increase in the permeate production and, consequently, in the gain-output ratio as per eq. (40). Thus, it is generally beneficial to operate at sub-atmospheric pressures in the air gap, as already noted in other studies [24–27].

One must bear in mind, however, that the total pressure within the

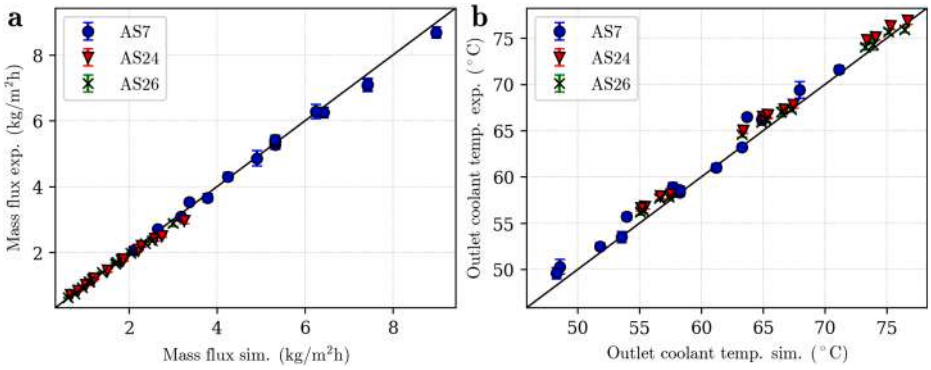

Fig. 5. Comparison of the results from the reduced model with experimental results reported by Andrés-Mañas et al. (2022) [33]. (a) Mass flux; (b) Cold feedwater temperature at the outlet.

Table 5
Operational parameters for the base case of the physical analysis.

Parameter	Value	Unit
$\dot{m}_{in}$, $\dot{m}_c$	400	[kg/h]
$T_{f,in}$	60	[°C]
$T_{c,in}$	25	[°C]
W_f, W_c	3.5	[wt%]
p_{vac}	500.0	[mbar]

air gap must be kept above the saturation pressure of the distillate to allow for it to condense and drip into the permeate tank instead of being lost in the vacuum line shown in Fig. 1. Moreover, excessively low air gap pressures may compromise the hydrophobicity and overall integrity of the membrane, leading to process degradation [28,32].

4.4. Number of feedwater channels

Fig. 7a shows the effect the number of hot and cold feedwater channels pairs has on the water productivity, i.e., the mass flux and permeate flow rate. A mild increase in both the mass flux and permeate flow rate through the membrane is predicted by lowering the number of channels from 20 to 2. A more pronounced effect occurs in the gain-output ratio (GOR), with up to a 50% increase when the number of channels is varied in the same range, as indicated by Fig. 7b. Given that the feedwater mass flow rate is fixed, less channels mean higher average velocities in each channel. However, to maintain the membrane area at the value prescribed by Table 1, the length of each channel must grow in the same proportion as the increase in velocity, thus keeping the feed-water residence time the same and excluding the reported effect it has of increasing the energy efficiency of spiral-wound V-AGMD modules [32]. The increase in velocity as the number of channels diminishes leads to

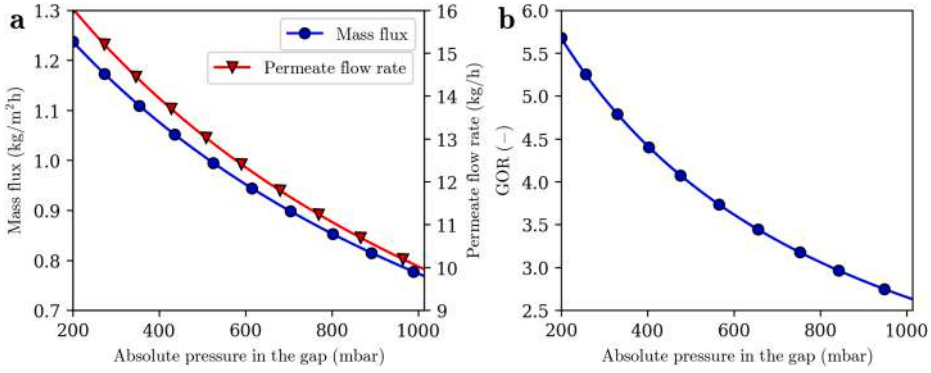

Fig. 6. Effect of the absolute air gap pressure in the performance of the V-AGMD desalination module. (a) Mass flux and permeate flow rate; (b) Gain-output ratio.

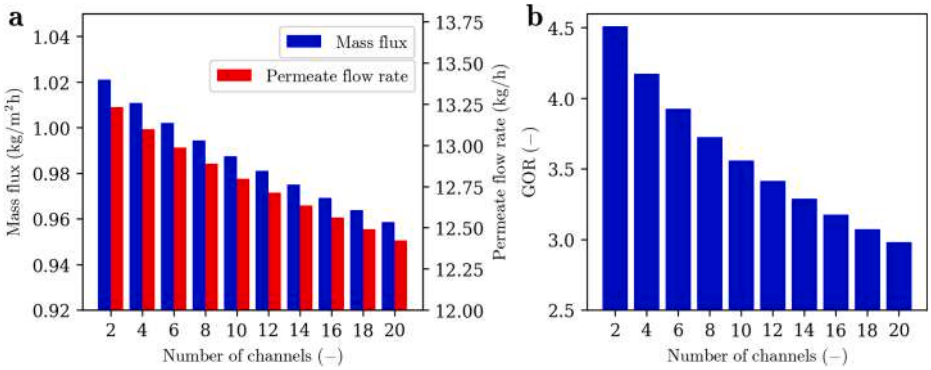

Fig. 7. Effect of the number of channels in the performance of the V-AGMD desalination module. (a) Mass flux and permeate flow rate; (b) Gain-output ratio.

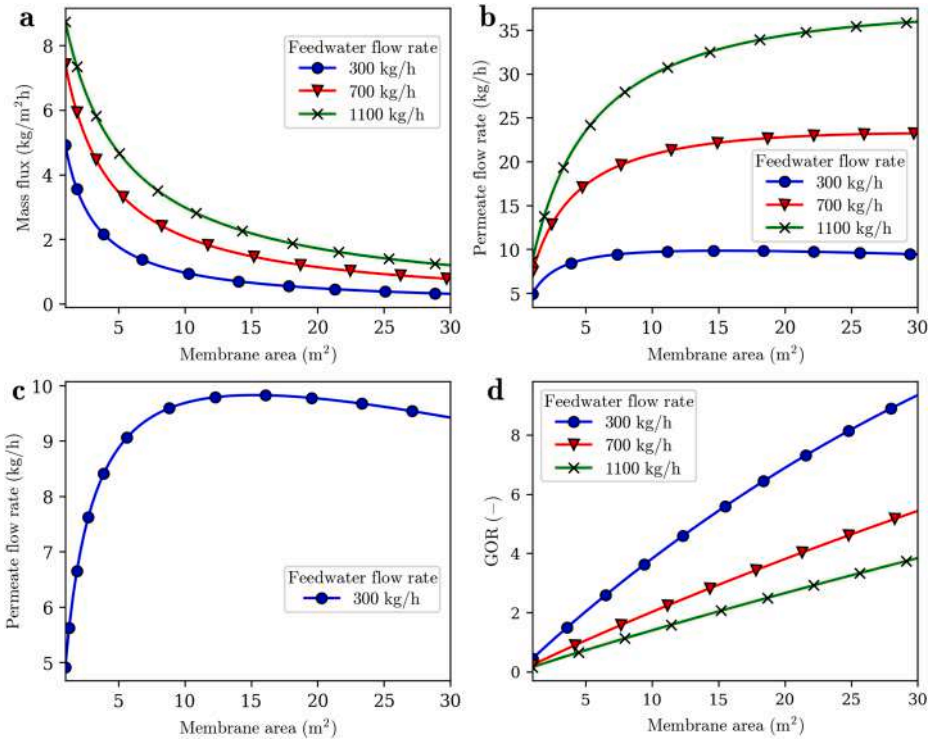

Fig. 8. Effect of the membrane area in the performance of the V-AGMD desalination module for different feedwater flow rates. (a) Mass flux; (b) permeate flow rate; (c) permeate flow rate for a feedwater flow rate of 300 kg/h; (d) Gain-output ratio.

higher Reynolds numbers and thus more effective convective heat transfer in the hot and cold feedwater channels, as predicted by eq (2a-d). In turn, the convective heat transfer enhancement increases the temperature polarization coefficient, TPC, i.e., the effective driving force for membrane distillation becomes closer to the maximum possible. Data provided in the Supplementary Information supports a direct relation between the gain-output ratio and the temperature polarization coefficient in the form GOR ≅ 8TPC, indicating that these two metrics are strongly correlated as the number of channels varies. The reason is that the lower convective-heat-transfer-related irreversibility leads to more effective use of the provided thermal energy input.

Caveats of lowering the number of feedwater channels are the increase in the pumping costs and the excessive membrane length that may be difficult to manufacture and/or assemble; the analysis of both side-effects is beyond the scope of this work.

4.5. Membrane area

Fig. 8a consistently shows that modules with higher total membrane area decrease the water mass flux through the membrane. Nevertheless, the permeate flow rate, depicted in Fig. 8b, since it is the result of the product between the mass flux and the membrane area, shows a different trend for low membrane areas, even though, it eventually saturates. One interesting feature of Fig. 8b, is that, for the lower feedwater mass flow rate (300 kg/h), an optimum membrane area for maximum permeate flow rate through the membrane is present for $A_m \sim 15\,m^2$, as made clear by Fig. 8c that provides a zoomed view of the curve for permeate flow rate versus the membrane area for this feedwater mass flow rate. The energy efficiency as measured by the gain-output ratio, on the other hand, monotonically increases with the membrane area according to the results in Fig. 8d. These observations are due to the tradeoff between transport-phenomena-related irreversibility and driving force. Increasing the membrane area lowers the temperature difference between the water free surfaces at the hot side of the membrane and the permeate, thereby decreasing the entropy generation of the heat and mass transfer and, at the same time, the partial pressure difference. As the membrane area grows, the driving force decreases to a point where the membrane area is not capable of offsetting the associated mass flux decrease, which is responsible for the existence of the maximum permeate flow rate value.

Furthermore, lower feedwater mass flow rate is detrimental to the water productivity and beneficial to the energy efficiency. This effect is due to the higher residence time, and is in line with what was reported for similar modules [32].

4.6. Module and operating conditions

Gathering the conclusions from the previous sections without the intent of formally optimizing the V-AGMD module, improvements in the base case established by the Tables 1 and 5 can be proposed just for illustration purposes. The number of feedwater channels is set to 4, to avoid excessive membrane and channel lengths, while still benefitting from the improvements predicted in Fig. 7. The feedwater mass flow rate and membrane are respectively set to 300 kg/h and 25.92 m^2 [32,33], and the absolute pressure in the air gap is considered to be 200 mbar. The permeate flow rate for this case is 11.7 kg/h. The gain-output ratio is 12.7, which is equivalent to a specific thermal energy consumption of 50.7 kWh(th)/m^3; such figures render the proposed module energetically competitive with multi-effect distillation (MED) [49]. In addition, the predicted GOR is markedly larger than the ones reported for similar pilot-scale DCMD systems that are below 2 [22].

5. Conclusion

A reduced, physics-based model for spiral-wound V-AGMD water desalination modules was proposed and implemented in an open-source computational code. An extensive validation campaign was conducted encompassing 86 experimental results from the module installed in the COPPE/UFRJ plant and others available in the open literature. Despite its simplicity, the numerical model was quite successful in predicting the

performance of the membrane distillation module, enabling its use as a tool for easy evaluation and optimization in different scenarios and of the integration with other equipment.

A physical analysis was conducted involving the effects of the absolute pressure in the air gap, number of feedwater channels, and membrane area in the water productivity and the energy efficiency of the membrane distillation module. Lower air gap pressure and number of feedwater channels are always found to improve the mass flux, the permeate flow rate through the membrane, and the gain-output ratio. These observations are respectively associated with the reduction of the mass transport resistance through the membrane and the air gap and the smaller temperature polarization that results from increases in fluid velocity within the channel. In turn, a more nuanced effect is associated with higher membrane areas that induce higher energy efficiency at the expense of lower mass fluxes. For a fixed feedwater flow rate, there exists an optimum membrane area above which it is not capable to offset the lower driving force and mass flux, despite improvements in the energy efficiency. Moreover, lower feedwater flow rates are shown to improve the energy efficiency, while demanding more modules to supply a given amount of water, because of longer feedwater residence times. With the acquired knowledge, a V-AGMD module with accompanying operational conditions was put forward and shown to be competitive with the more established distillation technology MED in energy consumption terms.

Future works involving a judicious comparison of V-AGMD, DCMD, and VMD operating at the pilot-scale are necessary to establish which configuration is preferable for efficient water desalination.

CRediT authorship contribution statement

Kleber Marques Lisboa: Writing – original draft, Visualization, Validation, Software, Project administration, Methodology, Investigation, Funding acquisition, Formal analysis, Conceptualization. **Ingrid Vasconcelos Curcino:** Writing – review & editing, Visualization, Validation, Methodology, Investigation, Formal analysis. **Abdul Orlando Cárdenas Gómez:** Writing – review & editing, Visualization, Validation, Methodology, Investigation, Formal analysis. **Luz Elena Peñaranda Chenche:** Writing – review & editing, Validation, Investigation, Formal analysis. **Renato Machado Cotta:** Writing – review & editing, Supervision, Funding acquisition. **Carolina Palma Naveira-Cotta:** Writing – review & editing, Supervision, Project administration, Funding acquisition.

Declaration of competing interest

The authors declare that they have no known competing financial interests or personal relationships that could have appeared to influence the work reported in this paper.

Acknowledgements

The authors are grateful for the financial support offered by Petrogal Brasil S.A. (Grant no. 38), ANP, EMBRAPII, and the Brazilian Government agencies CNPq, CAPES, and FAPERJ (Grants no. E-26/010/002590/2019, E-26/211.519/2021, and E-26/200.212/2023).

Appendix A. Supplementary data

Supplementary data to this article can be found online at https://doi.org/10.1016/j.seppur.2024.127891.

REFERENCES

[1] A. Alkhudhiri, N. Darwish, N. Hilal, Membrane distillation: A comprehensive review, Desalination 287 (2012) 2–18, https://doi.org/10.1016/j.desal.2011.08.027.

[2] E. Drioli, A. Ali, F. Macedonio, Membrane distillation: Recent developments and perspectives, Desalination 356 (2015) 56–84, https://doi.org/10.1016/j.desal.2014.10.028.

[3] A. Alkhudhiri, N. Darwish, N. Hilal, Treatment of high salinity solutions: Application of air gap membrane distillation, Desalination 287 (2012) 55–60, https://doi.org/10.1016/j.desal.2011.08.056.

[4] A. Alkhudhiri, N. Hilal, Air gap membrane distillation: A detailed study of high saline solution, Desalination 403 (2017) 179–186, https://doi.org/10.1016/j.desal.2016.07.046.

[5] J. Swaminathan, H.W. Chung, D.M. Warsinger, J.H. Lienhard V, Energy efficiency of membrane distillation up to high salinity: Evaluating critical system size and optimal membrane thickness, Appl. Energy 211 (2018) 715–734, https://doi.org/10.1016/j.apenergy.2017.11.043.

[6] N. Dow, S. Gray, J. Li, J. Zhang, E. Ostarcevic, A. Liubinas, P. Atherton, G. Roeszler, A. Gibbs, M. Duke, Pilot trial of membrane distillation driven by low grade waste heat: Membrane fouling and energy assessment, Desalination 391 (2016) 30–42, https://doi.org/10.1016/j.desal.2016.01.023.

[7] A. Yadav, P.K. Labhasetwar, V.K. Shahi, Membrane distillation using low-grade energy for desalination: A review, J. Environ. Chem. Eng. 9 (2021) 105818, https://doi.org/10.1016/j.jece.2021.105818.

[8] A. Deshmukh, M. Elimelech, Understanding the impact of membrane properties and transport phenomena on the energetic performance of membrane distillation desalination, J. Membr. Sci. 539 (2017) 458–474, https://doi.org/10.1016/j.memsci.2017.05.017.

[9] A. Deshmukh, C. Boo, V. Karanikola, S. Lin, A.P. Straub, T. Tong, D.M. Warsinger, M. Elimelech, Membrane distillation at the water-energy nexus: limits, opportunities, and challenges, Energy Environ. Sci. 11 (2018) 1177–1196, https://doi.org/10.1039/C8EE00291F.

[10] N. Ghaffour, T.M. Missimer, G.L. Amy, Technical review and evaluation of the economics of water desalination: Current and future challenges for better water supply sustainability, Desalination 309 (2013) 197–207, https://doi.org/10.1016/j.desal.2012.10.015.

[11] M. Elimelech, W.A. Phillip, The Future of Seawater Desalination: Energy, Technology, and the Environment, Science 333 (2011) 712–717, https://doi.org/10.1126/science.1200488.

[12] M.H. Sharqawy, J.H. Lienhard, S.M. Zubair, Thermophysical properties of seawater: a review of existing correlations and data, Desalination, Water Treat. 16 (2010) 354–380, https://doi.org/10.5004/dwt.2010.1079.

[13] R. Ullah, M. Khraisheh, R.J. Esteves, J.T. McLeskey, M. AlGhouti, M. Gad-el-Hak, H, Vahedi Tafreshi, Energy efficiency of direct contact membrane distillation, Desalination 433 (2018) 56–67, https://doi.org/10.1016/j.desal.2018.01.025.

[14] I.V. Curcino, B.S. Reis, A.O.C. Gomez, L.E.P. Chenche, J.A. Lima, C.P. Naveira-Cotta, R.M. Cotta, Experimental evaluation of solar desalination system with vacuum-enhanced air gap membrane distillaiton, in: Proceeding Int. Heat Transf. Conf. 17, Begellhouse, Cape Town, South Africa, 2023: p. 10. Doi: 10.1615/IHTC17.100-80.

[15] C.P. Naveira-Cotta, I.V. Curcino, B.S. Reis, A.O.C. Gomez, P.R.S. Costa Jr., J.D.C.G. Carvalho, L.E.P. Chenche, J.A. Lima, R.M. Cotta, A sustainable polycogeneration prototype for decentralized production of electricity, distilled water and biodiesel, in: Proceeding 8th Therm. Fluids Eng. Conf. TFEC, Begellhouse, College Park, USA, 2023: p. 703. Doi: 10.1615/TFEC2023.eet.047412.

[16] I.V. Curcino, T.R.P. Costa, G.O. Rosa, A.O. Cárdenas Gómez, C.P. Naveira-Cotta, R. M. Cotta, Experimental Analysis of the Desalination Process by Vacuum Enhanced Air Gap Membrane Distillation in a Pilot System, in: Proc. 27th Int. Congr. Mech. Eng. COBEM 2023, Florianópolis, SC, Brazil, 2023: p. 10.

[17] L. Eykens, T. Reyns, K. De Sitter, C. Dotremont, L. Pinoy, B. Van Der Bruggen, How to select a membrane distillation configuration? Process Conditions and Membrane Influence Unraveled, Desalination 399 (2016) 105–115, https://doi.org/10.1016/j.desal.2016.08.019.

[18] K. Marques Lisboa, D. Busson De Moraes, C. Palma Naveira-Cotta, R. Machado Cotta, Analysis of the membrane effects on the energy efficiency of water desalination in a direct contact membrane distillation (DCMD) system with heat recovery, Appl. Therm. Eng. 182 (2021) 116063, https://doi.org/10.1016/j.applthermaleng.2020.116063.

[19] V.T. Shahu, S.B. Thombre, Air gap membrane distillation: A review, J. Renew. Sustain. Energy 11 (2019) 045901, https://doi.org/10.1063/1.5063766.

[20] Y. Elhenawy, N.A.S. Elminshawy, M. Bassyouni, A. Alhathal Alanezi, E. Drioli, Experimental and theoretical investigation of a new air gap membrane distillation module with a corrugated feed channel, J. Membr. Sci. 594 (2020) 117461, https://doi.org/10.1016/j.memsci.2019.117461.

[21] A.S. Alsaadi, N. Ghaffour, J.-D. Li, S. Gray, L. Francis, H. Maab, G.L. Amy, Modeling of air-gap membrane distillation process: A theoretical and experimental study, J. Membr. Sci. 445 (2013) 53–65, https://doi.org/10.1016/j.memsci.2013.05.049.

[22] L. Eykens, I. Hitsov, K. De Sitter, C. Dotremont, L. Pinoy, B. Van der Bruggen, Direct contact and air gap membrane distillation: Differences and similarities between lab and pilot scale, Desalination 422 (2017) 91–100, https://doi.org/10.1016/j.desal.2017.08.018.

[23] M.-A.-E.-R. Abu-Zeid, Y. Zhang, H. Dong, L. Zhang, H.-L. Chen, L. Hou, A comprehensive review of vacuum membrane distillation technique, Desalination 356 (2015) 1–14, https://doi.org/10.1016/j.desal.2014.10.033.

[24] C. Guijt, G. Meindersma, T. Reith, A. Dehaan, Air gap membrane distillation1. Modelling and mass transport properties for hollow fibre membranes, Sep. Purif. Technol. 43 (2005) 233–244, https://doi.org/10.1016/j.seppur.2004.09.015.

[25] A.S. Alsaadi, L. Francis, H. Maab, G.L. Amy, N. Ghaffour, Evaluation of air gap membrane distillation process running under sub-atmospheric conditions:

Experimental and simulation studies, J. Membr. Sci. 489 (2015) 73–80, https://doi.org/10.1016/j.memsci.2015.04.008.
[26] M.-A.-E.-R. Abu-Zeid, L. Zhang, W.-Y. Jin, T. Feng, Y. Wu, H.-L. Chen, L. Hou, Improving the performance of the air gap membrane distillation process by using a supplementary vacuum pump, Desalination 384 (2016) 31–42, https://doi.org/10.1016/j.desal.2016.01.020.
[27] C. Guijt, G. Meindersma, T. Reith, A. Haan, Air gap membrane distillation2. Model validation and hollow fibre module performance analysis, Sep. Purif. Technol. 43 (2005) 245–255, https://doi.org/10.1016/j.seppur.2004.09.016.
[28] A. Ruiz-Aguirre, J.A. Andrés-Mañas, G. Zaragoza, Evaluation of Permeate Quality in Pilot Scale Membrane Distillation Systems, Membranes 9 (2019) 69, https://doi.org/10.3390/membranes9060069.
[29] I. Hitsov, L. Eykens, W.D. Schepper, K.D. Sitter, C. Dotremont, I. Nopens, Full-scale direct contact membrane distillation (DCMD) model including membrane compaction effects, J. Membr. Sci. 524 (2017) 245–256, https://doi.org/10.1016/j.memsci.2016.11.044.
[30] I. Hitsov, K. De Sitter, C. Dotremont, P. Cauwenberg, I. Nopens, Full-scale validated Air Gap Membrane Distillation (AGMD) model without calibration parameters, J. Membr. Sci. 533 (2017) 309–320, https://doi.org/10.1016/j.memsci.2017.04.002.
[31] J.A. Andrés-Mañas, L. Roca, A. Ruiz-Aguirre, F.G. Acién, J.D. Gil, G. Zaragoza, Application of solar energy to seawater desalination in a pilot system based on vacuum multi-effect membrane distillation, Appl. Energy 258 (2020) 114068, https://doi.org/10.1016/j.apenergy.2019.114068.
[32] J.A. Andrés-Mañas, I. Requena, G. Zaragoza, Characterization of the use of vacuum enhancement in commercial pilot-scale air gap membrane distillation modules with different designs, Desalination 528 (2022) 115490, https://doi.org/10.1016/j.desal.2021.115490.
[33] J.A. Andrés-Mañas, I. Requena, A. Ruiz-Aguirre, G. Zaragoza, Performance modelling and optimization of three vacuum-enhanced membrane distillation modules for upscaled solar seawater desalination, Sep. Purif. Technol. 287 (2022) 120396, https://doi.org/10.1016/j.seppur.2021.120396.
[34] J.A. Andrés-Mañas, I. Requena, G. Zaragoza, Membrane distillation of high salinity feeds: Steady-state modelling and optimization of a pilot-scale module in vacuum-assisted air gap operation, Desalination 553 (2023) 116449, https://doi.org/10.1016/j.desal.2023.116449.
[35] K.M. Lisboa, J.R.B. De Souza, C.P. Naveira-Cotta, R.M. Cotta, Heat and mass transfer in hollow-fiber modules for direct contact membrane distillation: Integral transforms solution and parametric analysis, Int. Commun. Heat Mass Transf. 109 (2019) 104373, https://doi.org/10.1016/j.icheatmasstransfer.2019.104373.
[36] A. Alklaibi, N. Lior, Transport analysis of air-gap membrane distillation, J. Membr. Sci. 255 (2005) 239–253, https://doi.org/10.1016/j.memsci.2005.01.038.
[37] A.M. Alklaibi, N. Lior, Comparative Study of Direct-Contact and Air-Gap Membrane Distillation Processes, Ind. Eng. Chem. Res. 46 (2007) 584–590, https://doi.org/10.1021/ie051094u.
[38] I.V. Curcino, P.R.S.C. Júnior, A.O.C. Gómez, L.E.P. Chenche, J.A. Lima, C. P. Naveira-Cotta, R.M. Cotta, Analysis of effective thermal conductivity and tortuosity modeling in membrane distillation simulation, Micro Nano Eng. 17 (2022) 100165, https://doi.org/10.1016/j.mne.2022.100165.
[39] R.W. Field, H.Y. Wu, J.J. Wu, Multiscale Modeling of Membrane Distillation: Some Theoretical Considerations, Ind. Eng. Chem. Res. 52 (2013) 8822–8828, https://doi.org/10.1021/ie302363e.
[40] K.W. Lawson, D.R. Lloyd, Membrane distillation, J. Membr. Sci. 124 (1997) 1–25, https://doi.org/10.1016/S0376-7388(96)00236-0.
[41] Ó. Andrjesdóttir, C.L. Ong, M. Nabavi, S. Paredes, A.S.G. Khalil, B. Michel, D. Poulikakos, An experimentally optimized model for heat and mass transfer in direct contact membrane distillation, Int. J. Heat Mass Transf. 66 (2013) 855–867, https://doi.org/10.1016/j.ijheatmasstransfer.2013.07.051.
[42] A. Bejan, Convection heat transfer, Fourth edition, Wiley, Hoboken, New Jersey, 2013.
[43] S. Lin, N.Y. Yip, M. Elimelech, Direct contact membrane distillation with heat recovery: Thermodynamic insights from module scale modeling, J. Membr. Sci. 453 (2014) 498–515, https://doi.org/10.1016/j.memsci.2013.11.016.
[44] K.G. Nayar, M.H. Sharqawy, L.D. Banchik, J.H. Lienhard V, Thermophysical properties of seawater: A review and new correlations that include pressure dependence, Desalination 390 (2016) 1–24, https://doi.org/10.1016/j.desal.2016.02.024.
[45] P.T. Tsilingiris, Review and critical comparative evaluation of moist air thermophysical properties at the temperature range between 0 and 100 °C for Engineering Calculations, Renew. Sustain. Energy Rev. 83 (2018) 50–63, https://doi.org/10.1016/j.rser.2017.10.072.
[46] S. Balay, S. Abhyankar, M. Adams, S. Benson, J. Brown, P. Brune, K. Buschelman, E. Constantinescu, L. Dalcin, A. Dener, V. Eijkhout, J. Faibussowitsch, W. Gropp, V. Hapla, T. Isaac, P. Jolivet, D. Karpeev, D. Kaushik, M. Knepley, F. Kong, S. Kruger, D. May, L. McInnes, R. Mills, L. Mitchell, T. Munson, J. Roman, K. Rupp, P. Sanan, J. Sarich, B. Smith, S. Zampini, H. Zhang, H. Zhang, J. Zhang, PETSc/TAO Users Manual (Rev. 3.19), 2023. Doi: 10.2172/1968587.
[47] Y. Saad, M.H. Schultz, GMRES: A Generalized Minimal Residual Algorithm for Solving Nonsymmetric Linear Systems, SIAM J. Sci. Stat. Comput. 7 (1986) 856–869, https://doi.org/10.1137/0907058.
[48] B. Weidenfeller, M. Höfer, F.R. Schilling, Thermal conductivity, thermal diffusivity, and specific heat capacity of particle filled polypropylene, Compos. Part Appl. Sci. Manuf. 35 (2004) 423–429, https://doi.org/10.1016/j.compositesa.2003.11.005.
[49] A. Cipollina, M.G. Di Sparti, A. Tamburini, G. Micale, Development of a Membrane Distillation module for solar energy seawater desalination, Chem. Eng. Res. Des. 90 (2012) 2101–2121, https://doi.org/10.1016/j.cherd.2012.05.021.